machines

MDPI

Article

A New Single-Leg Lower-Limb Rehabilitation Robot: Design, Analysis and Experimental Evaluation

Hongfei Yu [1,2], Siyuan Zheng [3], Jiantao Wu [1,2], Li Sun [1,2,*], Yongliang Chen [3,*], Shuo Zhang [1] and Zhongzhi Qin [1]

[1] School of Art and Design, Yanshan University, Qinhuangdao 066004, China
[2] Intelligent Industrial Design Technology Innovation Center of Hebei Province, Yanshan University, Qinhuangdao 066004, China
[3] Parallel Robot and Mechatronic System Laboratory of Hebei Province, School of Mechanical Engineering, Yanshan University, Qinhuangdao 066004, China
* Correspondence: sunli@ysu.edu.cn (L.S.); chenyongliang0126@outlook.com (Y.C.)

Abstract: Conventional lower-limb rehabilitation robots are large, complicated to wear, and require moving the patient to a designated position. To solve these problems, a new single-legged lower-limb rehabilitation robot (S-LLRR) that is easy to move and suitable for different height carriers was proposed. The mechanical leg has a variable working space, and its rotating joints are designed with mechanical limiters. The series configuration of the S-LLRR was analyzed, and trajectory planning was performed based on continuous linear motion training. Meanwhile, an active training control method based on the sand model was proposed to enhance the motion sensation of patients, and an active participation degree evaluation model was designed based on human physiological information. The simulation and experimental results showed that S-LLRR had a large workspace and good motion accuracy, and the accuracy of the active participation degree evaluation model could reach more than 85%. This research could provide a theoretical basis for improving the standardization and compliance of lower-limb robot rehabilitation training.

Keywords: lower-limb rehabilitation robot; trajectory planning; active training control; active participation

check for updates

Citation: Yu, H.; Zheng, S.; Wu, J.; Sun, L.; Chen, Y.; Zhang, S.; Qin, Z. A New Single-Leg Lower-Limb Rehabilitation Robot: Design, Analysis and Experimental Evaluation. *Machines* **2023**, *11*, 447. https://doi.org/10.3390/machines11040447

Academic Editor: Dan Zhang

Received: 22 February 2023
Revised: 19 March 2023
Accepted: 27 March 2023
Published: 2 April 2023

Copyright: © 2023 by the authors. Licensee MDPI, Basel, Switzerland. This article is an open access article distributed under the terms and conditions of the Creative Commons Attribution (CC BY) license (https://creativecommons.org/licenses/by/4.0/).

1. Introduction

Aging, accidents, and environmental pollution increase the risk of developing neurological brain injury diseases. Stroke is a common acquired brain injury disease, with a significant increase in the number of deaths or disabilities due to stroke each year, and often leads to long-term limb dysfunction, especially hemiplegia and hemiparesis, after treatment [1,2]. Clinical studies have shown that repetitive and effective rehabilitation of the disabled limb is essential to avoid disuse atrophy of the muscles and to promote the repair of the patient's nervous system and recovery of motor function [3,4].

Rehabilitation of the lower extremities is essential for restoring gait performance and daily activities in stroke patients [5]. With the in-depth integration of rehabilitation medicine and robotics, many models of lower-extremity rehabilitation robots have been designed. Hocoma of Switzerland developed Lokomat, a suspended gait training lower-limb rehabilitation robot with multiple training modes and functional modules, including an optional FreeD module to guide lateral translation and lateral rotation of the pelvis during training [6]. Yildiz University of Science and Technology created a sitting-lying gait trainer, Physiotherabot, that could learn specific motor movements through a robotic hand and perform rehabilitation movements without a physical therapist (PT) through a human-machine interface [7]. Wuhan Polytechnic University designed a lower-limb rehabilitation robot, combining a frame structure and a vertical vibration module that could simulate gait movements and excite the neuromuscular system for the corresponding rehabilitation function [8]. In some research, in order to avoid the secondary injury caused by the rigid structure, the flexible structure was considered in the design of the lower-limb rehabilitation

robot [9]. Harbin Engineering University proposed a hybrid robot composed of a rigid mobile device and a flexible drive system that could realize adduction or abduction and internal or external rotation in lower-limb movement training [10]. The Federal University of Uberlândia proposed an actuated cable-driven lower-limb rehabilitation robot that was composed of a fixed base, a movable platform, and a mobile platform that could connect up to six cables while performing separate motions of the hip, knee, and ankle [11]. However, the abovementioned lower-limb rehabilitation robots occupy a large space, which is not suitable for home use, and there will be difficulties in their use when patients with stroke are not able to move in the early stage. To address this deficiency, the LR2 lowe- limb rehabilitation robot developed by Yaskawa Electric Corporation of Japan could be easily combined with wheelchairs and beds, connecting the patient's calves and ankles with the mechanism, and could perform various training modes, such as single-joint training motion, multijoint coupling motion, and mixed motion [12]. Yanshan University developed a terminal traction type lower-limb rehabilitation robot based on hybrid mechanisms (HE-LRR), which had the advantages of a compact structure and a large working space, and was suitable for the rehabilitation needs of the patients in the acute phase [13]. However, due to the small contact between the terminal traction robot and the body of the patient, no restrictions on lower-limb movements will be made, resulting in deviation from the preset training trajectory during training [14]. On the other hand, the success of physical therapy and rehabilitation depends mostly on the continuity of the exercises. Kocaeli University created a low-cost and portable wrist rehabilitation robot (POWROBOT) that could be used both at home and in physical therapy centers [15]. Calabria University designed a novel bionic robotic device for upper-limb rehabilitation tasks at home that could be easily portable and managed remotely by a professional therapist [16]. Some studies have concluded that rehabilitation robots are as effective as conventional therapy, but their cost-effectiveness is preventing their uptake [17]. Therefore, reducing the manufacturing cost and increasing the mobility of their rehabilitation robots is very beneficial for their application.

As people's demands for rehabilitation efficiency and rehabilitation services are increasing, the design of inspiring patients' active participation in the training process is becoming more and more important [18]. Bath University developed a multigait trainer, established a multimode human-computer interaction system (HRI), to enhance the subjects' active participation in the gait rehabilitation process, and could control the robot through the active motion intention of users [19]. The University of Shanghai for Science and Technology proposed an active training strategy for lower-limb rehabilitation robots based on a spring-damping model, using a force-sensing control method based on human-computer interaction to effectively improve the participation and efficiency of rehabilitation training [20]. In addition, the use of human physiological information has been proven to be an effective method for controlling rehabilitation and assisting devices, which can effectively improve the rehabilitation effect of the robot by combining bioelectric signals, such as electromyography, when establishing the lower-limb rehabilitation robot system [21–23].

Based on the above research and analysis, this study proposes a new single-legged lower-limb rehabilitation robot (hereinafter referred to as S-LLRR) that is easy to move and suitable for different height carriers to meet the rehabilitation needs of patients. This innovative mechanism design of S-LLRR makes it different from other lower-limb rehabilitation robots. The mechanical structure comparison with other lower-limb devices is shown in Table 1.

In the early rehabilitation stage of stroke patients, lower-limb training in sitting/lying posture can reduce the weight burden on the hips and legs of patients and increase the range of motion of lower-limb joints [24]. On this basis, the exoskeleton robot is conducive to improving the stability of rehabilitation training. Single-legged rehabilitation robots have simpler structures and lower manufacturing costs than two-legged ones. Therefore, this research has the following highlights: (1) A single-leg lower-limb rehabilitation robot with a compact structure, convenient movement, low manufacturing cost, and adjustable

mechanical leg has been designed, which can be combined with the vehicle in daily use to carry out rehabilitation training in sitting and lying positions. (2) An active training control strategy based on the sand model is designed to reconstruct the patients' environmental perception ability. Additionally, an evaluation model of active participation based on human physiological information is proposed to provide more effective rehabilitation training for patients.

Table 1. Mechanical structure comparison with other lower-limb rehabilitation robots.

Features	S-LLRR	Lokomat	Physiotherabot	LR2	HE-LRR
Type	Exoskeleton	Exoskeleton	Exoskeleton	Terminal traction	Terminal traction
Size	Moderate	Large	Large	Moderate	Moderate
Single leg/Double legs	Single	Double	Double	Single	Double
Leg length adjustment method	By motor	By hand	By hand	×	×
Posture	Sitting and lying	Standing	Sitting	Lying	Sitting and lying
Usage patterns	Combined with vehicle	Fixed position	Fixed seat	Combined with vehicle	Combined with vehicle
Manufacturing cost	Lower	Higher	Higher	Lower	Lower
Mobility	Easy	Harder	Harder	Easy	Easy

This paper first introduces the mechanical structure and control system of the S-LLRR. Secondly, based on continuous linear motion training, the trajectory planning of the rehabilitation robot is carried out, and an active training control strategy based on the sand model and an active involvement degree evaluation model based on physiological signals are designed. Finally, the working space of the rehabilitation robot is simulated, and the terminal trajectory tracking experiment and fatigue degree prediction experiment are carried out to verify the motion performance of the S-LLRR and the accuracy of the active involvement degree evaluation model.

2. Materials and Methods

2.1. Mechanical Design

Based on integrated design concept, the S-LLRR is mainly composed of control cabinet, lifting mechanism, and mechanical leg, as shown in Figure 1. The control cabinet and lifting mechanism are integrated into the frame to reduce size, and the wheels are installed at the bottom for easy movement. The mechanical leg is installed outside the frame, and patients can put their feet on the pedal and be bound by the velcro binding belt. After adjusting the appropriate height and length of the mechanical leg, the man-machine cooperative rehabilitation training can be performed in a lying or sitting position.

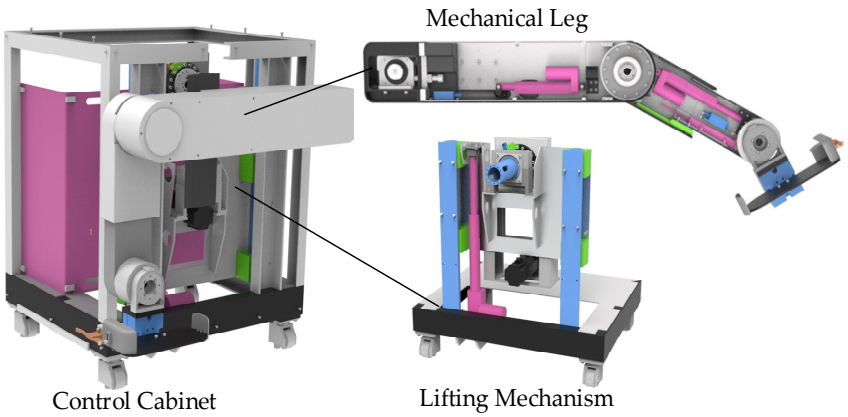


Figure 1. Mechanism of lower-limb rehabilitation robot.

2.1.1. Lifting Mechanism and Hip Joint Assembly Design

The lifting mechanism is an important component connecting the control cabinet and the mechanical leg. The hip joint assembly is mounted on two sets of vertical guides, and an electric actuator vertically installed on the base of the control cabinet is used to adjust the height of the mechanical leg relative to the ground. This design ensures that the mechanical leg can adapt to different height vehicles to eliminate the need for a rehabilitation chair, which reduces the cost of the robot and simplifies the boarding steps of postoperative stroke patients. Additionally, it is noteworthy that the lifting system is designed in the control cabinet to avoid contact with patients.

In the hip joint assembly shown in Figure 2, the motor is installed at the lower part and connected to the reducer through a belt drive. The thigh part is driven to rotate around the rotation axis at a reasonable rotational speed. Adjusting the height of the mechanical leg changes the position of the hip joint shaft relative to the ground, and the entire hip joint assembly moves up and down together with the mechanical leg.

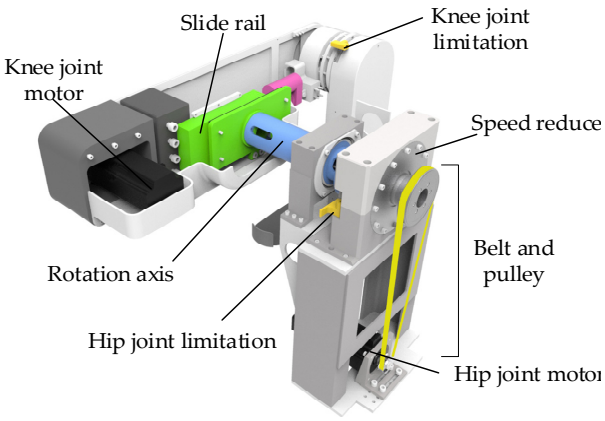


Figure 2. Hip joint assembly of rehabilitation mechanical leg.

2.1.2. Exoskeleton Mechanical Leg Structural Design

The mechanical leg is composed of three parts: thigh, calf, and ankle-foot, which are interconnected with each other through knee joint assembly and ankle joint assembly, and connected with the lifting mechanism through hip joint assembly. The function of the thigh part is to cooperate with the hip joint of the lower limb of the human body to create corner motion. The function of the thigh part is to cooperate with the human lower-limb hip joint to perform corner movements, while the length of the thigh part needs to be adjusted to meet personalized needs. Therefore, a slider and slide rail structure are designed in the middle of the thigh part, and the hip joint rotation shaft is connected to a horizontally movable slider to drive the thigh part to rotate; the electric push rod inside the mechanical leg cavity is installed on the slide rail to adjust the distance between the knee joint pivot point and the hip joint pivot point, as shown in Figure 2. The knee joint motor and balanced weight are designed at the end of the thigh part, and the power is transmitted to the knee joint reducer through the motor pulley and transmission belt, as shown in Figure 3.

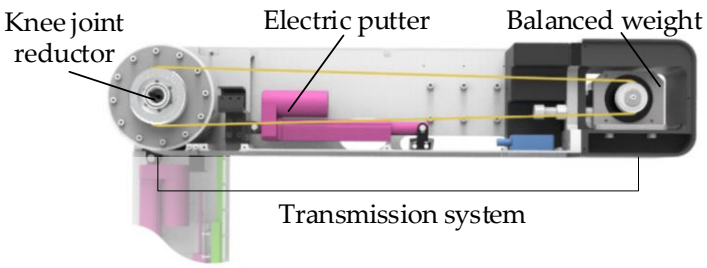


Figure 3. Thigh and transmission components of knee joint.

As can be expected, the synchronous slide and electric actuator are installed inside the calf part to make it telescopic, and it is connected to the thigh section through the knee reducer, as shown in Figure 4. The ankle-foot part of the rehabilitation robot is composed of the ankle joint drive assembly and the foot pedal assembly. The torque motor at the ankle joint drives the rotation of the foot pedal, which can collaborate with the patient to perform the rehabilitation training in the sagittal plane of the ankle joint, as shown in Figure 5.

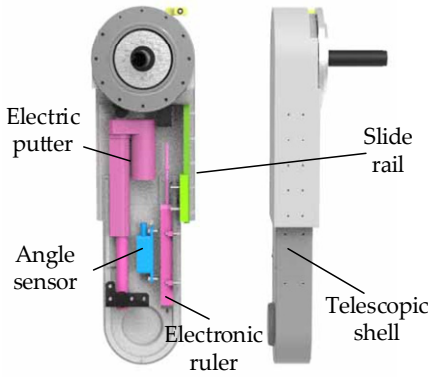


Figure 4. Calf adjustable mechanism.

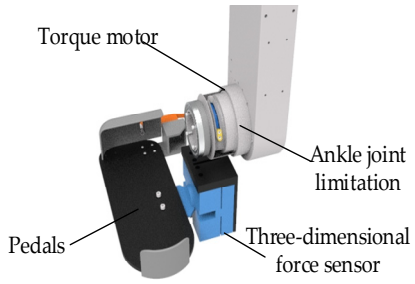


Figure 5. Foot and ankle components.

2.1.3. Limit Block and Limit Chute Design

In the movement of human lower limbs, extreme joint movements should be avoided as much as possible. Therefore, in order to ensure the safety of patients, it is necessary to install a limit position device on the rotating joint of the mechanical leg. According to the anteflexion amplitude of the human hip joint in the sagittal plane, the range of motion of the lower-limb rehabilitation robot is set from 0° to 140° for the hip joint, from 0° to 150° for the knee joint, and from 0° to 65° for the ankle joint [25,26]. On the other hand, realistic training needs require that the rehabilitation robot with a single robot leg structure has the function of bilateral lower-limb exchange training. The movable limit structures are designed at the joint of the mechanical leg, which can enable patients to switch between left and right leg rehabilitation training.

The bearing seat at the upper end of the hip joint drive assembly is designed with three structures: fixed limit block, moving limit block, and sliding limit block. The sliding limit block can be opened counterclockwise to slide to the A or B limit slot. When the lower-limb rehabilitation robot is used for the left (right) leg rehabilitation training, the moving limit block is located in the A (B) limit slot and works with the upper (lower) fixed limit block to achieve the angle limit of the moving limit block in the range of motion, as shown in Figure 6. Similarly, the limiting chute is also designed at the knee joint and ankle joint of the machine leg, and the left or right lower-limb rehabilitation training mode can be switched by moving the limiting block at the position of the chute, which will not be repeated here.

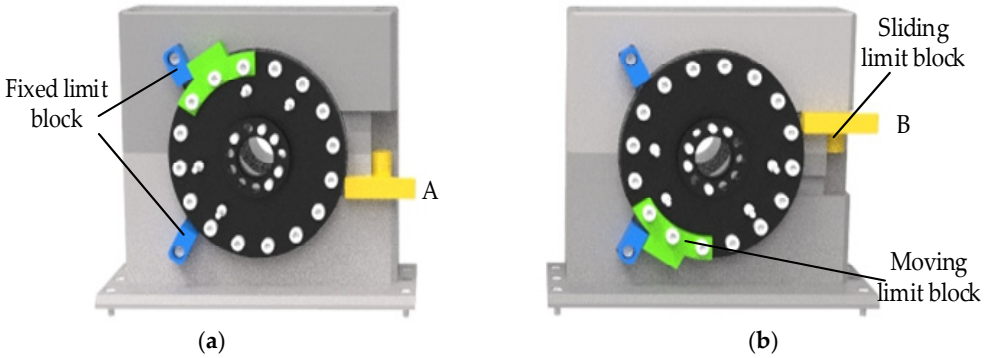


Figure 6. Schematic diagram of hip joint stopper. (**a**) The limit device for left leg rehabilitation training. (**b**) The limit device for right leg rehabilitation training.

Additionally, other innovative designs should be noted that belt transmission is used at both the hip joint and knee joint, which can effectively mitigate the impact and absorb vibration. Additionally, when unexpected situations cause joint torque overload, slippage between the belt and the pulley can play a certain protective role. Designing a knee joint servo motor and counterweight at the end of the thigh mechanism can balance the weight of the lower leg and ankle foot, reduce the load on the hip joint motor, and improve the dynamic performance of the mechanical leg. At the same time, the length adjustment device of the mechanical leg can adapt to the lower-limb length of people with a height of 1500–1900 mm.

2.2. Sensor and Control System Design

Human-machine interaction is essential in rehabilitation robots, ensuring safety and enhancing device control performance. Force sensors are the main components of human-machine interaction, which can provide effective interactive feedback between patients and rehabilitation devices [27]. Obtaining biological information directly from patients can also help solve human- machine interaction problems [28]. The S-LLRR usage process and control system are shown in Figure 7. The ankle joint force $\boldsymbol{F}_{\mathrm{m}}$ measured by the sensor and the leg rotation angle $\boldsymbol{P}_{\mathrm{m}}$ are processed by a control method to generate a position command $\boldsymbol{P}_{\mathrm{d}}$ and a speed command $\boldsymbol{V}_{\mathrm{d}}$, which drive the actuator to achieve position control. Passive training uses conventional PID control, and active training will be described in the next section. The physiological information of the human body can be evaluated for active participation, and then personalized rehabilitation training goals can be formulated.

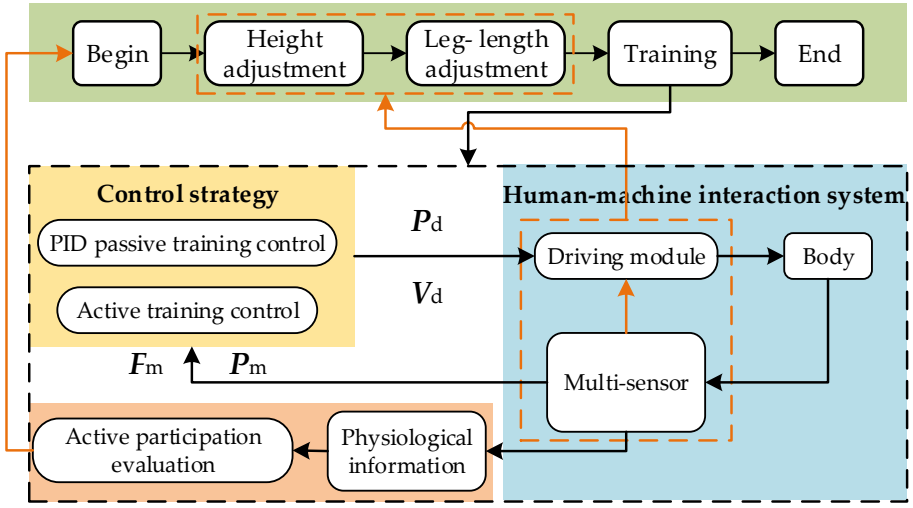


Figure 7. S-LLRR usage process and control flow chart.

The control system of lower-limb rehabilitation robot is mainly divided into four parts: interactive end, control center, acquisition card, actuator, and sensor, including upper computer, digital signal 2321 acquisition card, analog signal 8602 acquisition card, relay switch, USB/CAN communication module box, torque sensor, a set of three-dimensional ankle joint sensor, three sets of servo motor, three sets of electric push rod, two sets of electronic ruler, proximity switch, and multiple encoders, etc., as shown in Figure 8. The thigh angle sensor (BWK216S, Beiwei Information, Wuhan, China, Precision 0.2°) and the hip joint angle encoder (HKT3006, Ruipu Anhua, Jining, China) judge the hip joint motion angle. The electronic ruler (KTC2, Miran Technology, Shenzhen, China, Repetitiveness 0.01 mm) installed inside the shell can measure the telescopic travel of the mechanical leg. The calf angle sensor and the knee joint angle encoder can be used to judge the knee joint motion angle; three-dimensional force sensor (T501, Rieter, Changzhou, China, Repetitiveness 0.2%F.S.) and angle sensor are installed at the side end of the foot pedal assembly, which can collect the pressure data and angle information of the patient's foot, which is the basis for force feedback and position feedback.

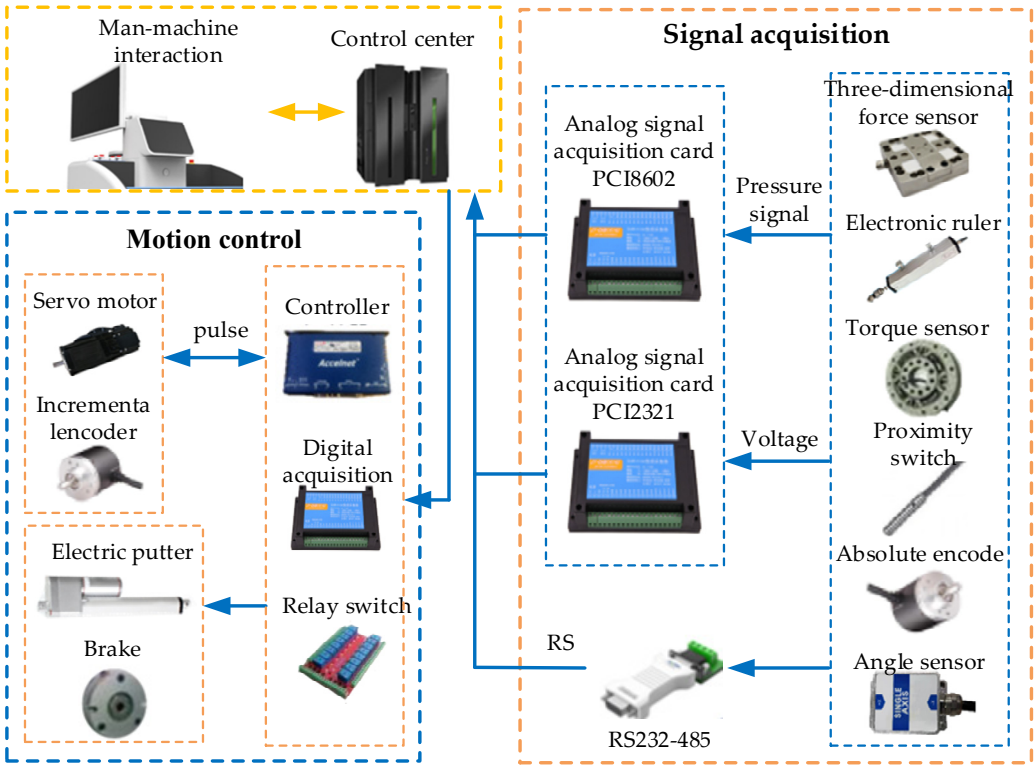


Figure 8. Hardware relation block diagram of control system.

When patients are undergoing rehabilitation training, the control center sends out control signals to control the motion of servo motor and electric push rod, respectively, through USB/CAN communication module box, driver, digital acquisition card, and relay, so as to realize the motion of each joint of the lower-limb rehabilitation robot. During the rehabilitation movement of the patient, the parameters such as the rotation angle and torque of the rehabilitation robot joint are monitored in real time through the three-dimensional force sensor, electronic ruler, torque sensor and angle sensor, etc. The measured parameters are fed back to the control center through the signal acquisition card and communication module, so that the whole system forms a closed-loop control system, and the real-time monitoring and adjustment of the patient's rehabilitation status by the medical staff at the interactive control end is realized.

3. Trajectory Planning and Control Strategy

3.1. Kinematic Analysis

After fixing the lifting mechanism and mechanical leg length adjustment device, the S-LLRR can be simplified as a three-degree-of-freedom serial mechanism. The coordinate system is established with the hip joint as the origin, as shown in Figure 9. l_1, l_2, and l_3 are the length of each part of the linkage, C_1, C_2, and C_3 are the centroid of the linkage, R_1, R_2, and R_3 are the distance from the centroid of the linkage to the joint, θ_1, θ_2, and θ_3 are the angular displacement of each part of the linkage, and P is the end point of the linkage.

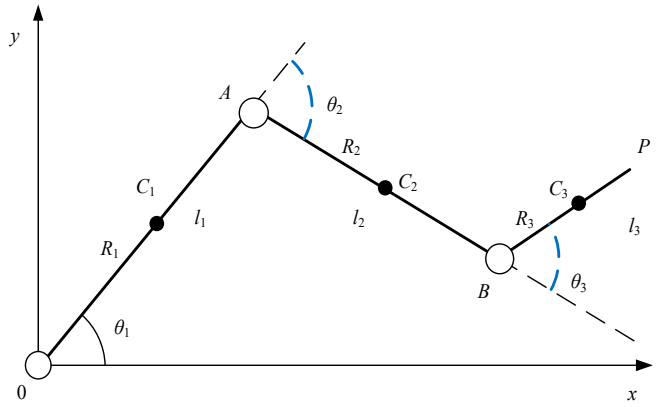


Figure 9. Connecting rod coordinate system.

The length variation range of linkage l_1 is specified as 360~460 mm and the angle variation range θ_1 is 0~135°; the length variation range of linkage l_2 is 320~420 mm and the angle variation range θ_2 is −150~0°; the length of linkage l_3 is 100 mm and the angle variation range θ_3 is −35~50°. The geometric relationship between the end position of the S-LLRR mechanical leg, the length and angle of each joint is obtained using the geometric method as follows:

$$\begin{cases} x_p = l_1 \cos\theta_1 + l_2 \cos(\theta_1 + \theta_2) + l_3 \cos(\theta_1 + \theta_2 + \theta_3) \\ y_p = l_1 \sin\theta_1 + l_2 \sin(\theta_1 + \theta_2) + l_3 \sin(\theta_1 + \theta_2 + \theta_3) \\ \alpha = \theta_1 + \theta_2 + \theta_3 \end{cases} \quad (1)$$

3.2. Rehabilitation Robot Training Trajectory Planning

The mainstream rehabilitation movements studied are a range of motion (ROM) rehabilitation training, linear rehabilitation training based on continuous passive motion (hereinafter referred to as CPM) and MOTOmed rehabilitation training [29,30]. Since CPM rehabilitation training not only can provide linked rehabilitation movements for hip, knee, and ankle joints, but also has relatively stable motion trajectories, which is the most accepted rehabilitation movement mode in lower-limb rehabilitation training at present [31]. Therefore, this paper takes CPM as an example to analyze the S-LLRR end motion trajectory. The end track of CPM is that the ankle axis maintains a straight motion in the working space. As shown in Figure 10, the ankle axis passes from the initial position B_1 through the middle position B to the end position B_2, and the knee position passes from the initial position A_1 through the middle position A to the end position A_2.

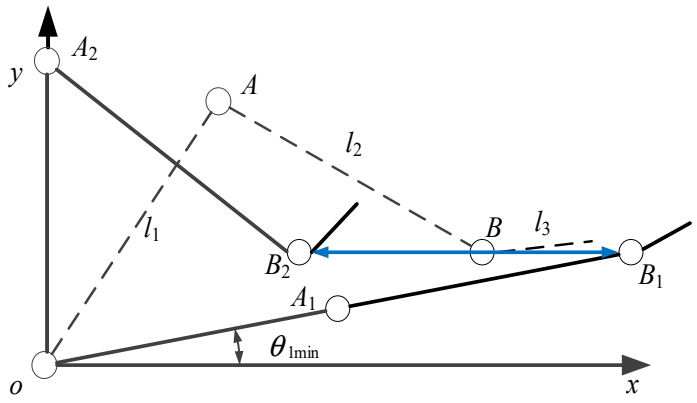


Figure 10. Trajectory of CPM end for rehabilitation robot.

According to the geometric relationship, the expression of the linear motion trajectory of the ankle joint center point B can be obtained as follows:

$$\begin{cases} y_B = (l_1 + l_2)\sin\theta_{1\min} \\ (l_1\cos\theta_{1\max} + l_2\cos(\theta_{1\max} + \theta_{2\min}) \le x_B \le (l_1 + l_2)\cos\theta_{1\min}) \end{cases} \tag{2}$$

Additionally, the kinematic inverse solution is performed to obtain the equations of motion of the hip and knee joints:

$$\begin{cases} \theta_1 = \arccos\left(\frac{x_B}{l_1^2+l_2^2+2l_1l_2\cos\theta_2}\right) - \arccos\left(\frac{l_2\cos\theta_2}{l_1^2+l_2^2+2l_1l_2\cos\theta_2}\right) \\ \theta_2 = \arccos\left(\frac{{x_B}^2+{y_B}^2-l_1^2-l_2^2}{2l_1l_2}\right) \end{cases} \tag{3}$$

The trajectory planning of S-LLRR in joint space is carried out using the cubic polynomial interpolation method. In order to meet the stable and stable motion, the static state of the starting point and the end point is required, that is, the speed and displacement are constrained. If the start time is t_0 and the end time is t_f then, the function expression of $\theta(t)$ is:

$$\theta(t) = a_0 + a_1t + a_2t^2 + a_3t^3 \tag{4}$$

Its acceleration and acceleration can be expressed as:

$$\begin{cases} \dot{\theta}(t) = a_1 + 2a_2t + 3a_3t^2 \\ \ddot{\theta}(t) = 2a_2 + 6a_3t \end{cases} \tag{5}$$

The constraints are as follows:

$$\begin{cases} \theta(t_0) = \theta_0 \\ \dot{\theta}(t_0) = 0 \\ \theta(t_f) = \theta_f \\ \dot{\theta}(t_f) = 0 \end{cases} \tag{6}$$

The coefficients can be obtained by bringing in Equations (4) and (5). Additionally, when the center point of the ankle joint is at the B_1 position, $\theta_{1\min} = 10^\circ$ and $\theta_2 = 0$, and when it is at the B_2 position, $x_{B_2} = 300$ mm, the movement time from B_1 to B_2 is 10 s. The motion curves of the hip and knee joints are obtained after simulation and analysis, using MATLAB, as shown in Figure 11. θ, $\dot{\theta}$, and $\ddot{\theta}$ represent the angular displacement, acceleration, and angular acceleration, respectively. It can be seen from the figure, the variation range of θ is within the normal range of human joint activities and the curves of $\dot{\theta}$ and $\ddot{\theta}$ are smooth and without mutation, which proves that the trajectory planning equation is reasonable.

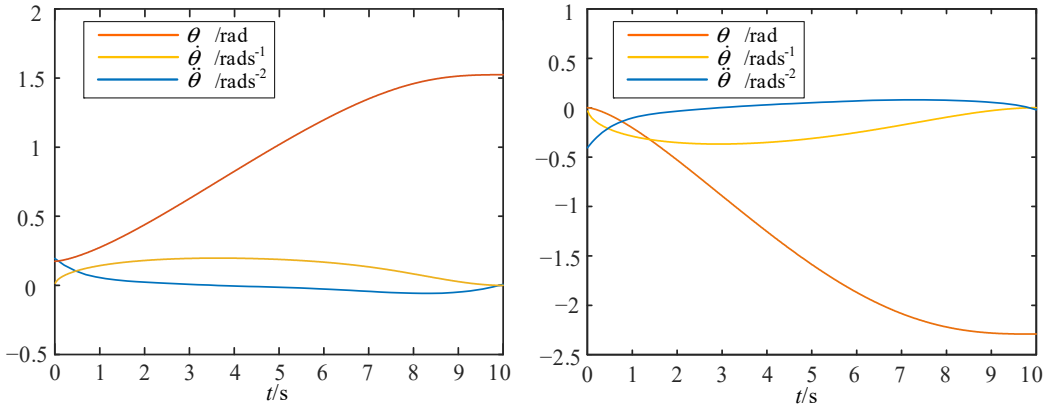


Figure 11. CPM principal rehabilitation movement simulation curve. (**a**) The simulation curve of hip joint. (**b**) The simulation curve of knee joint.

3.3. Active Training Control System Design

The research on the control strategy of the rehabilitation robot is an important part of realizing human-robot interaction for lower-limb rehabilitation robots. When a patient regains a certain degree of motor ability in the lower limb, the rehabilitation training with active participation of motor intention is required [32]. This paper studies the control strategy based on the sand model, which is intended to make the patient reconstruct the sense of movement in the special environment during active training. The sand model uses the relationship between stress and strain of sand bearing characteristics under vertical load to control the interactive forces of active training for patients. The empirical sand bearing model is shown as follows:

$$\begin{cases} p = (k_1 + bk_2)\left(\frac{l}{b}\right)^n \\ \boldsymbol{F} = pA \end{cases} \tag{7}$$

In the formula, p is the pressure per unit area, b is the radius of the short side or circular plate of the bearing plate, l is the amount of sagging, $\boldsymbol{F}$ is the vertical load acting on the pressure plate, A is the bearing area, n, k_1, and k_2 are a set of dimensionless constants characterizing the soil characteristics for sandy soil $k_1 = 0$. Therefore, the equation can be simplified by the relationship between the amount of sagging and the vertical force acting as:

$$l = b\left(\frac{\boldsymbol{F}}{Abk_2}\right)^{\frac{1}{n}} \tag{8}$$

Considering that the plantar force F_a is nonvertical with the ground when the patient uses the lower-limb rehabilitation robot, as shown in Figure 12. Therefore, the sagging amount is decomposed in the direction of the x-axis and y-axis. θ_a represents the angle between the patient force F_a and the x-axis in the sand experiment, l_a is the sagging amount of the sand model in the same force direction, and l_{a1} and l_{a2} are the sagging amount components, respectively.

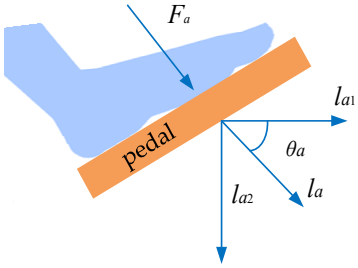


Figure 12. Sand model of active control strategy.

The control block diagram of the active training sand model was built, as shown in Figure 13. The sagging amount l_a is calculated from the patient force F_a in the sand model, and then the sagging amount l_a is decomposed into two directions of the x-axis and the y-axis, and the position inverse solution is carried out to obtain the desired position of the mechanical leg joint θ_q. The position controller is used to control the end of the mechanical leg to complete the sagging motion.

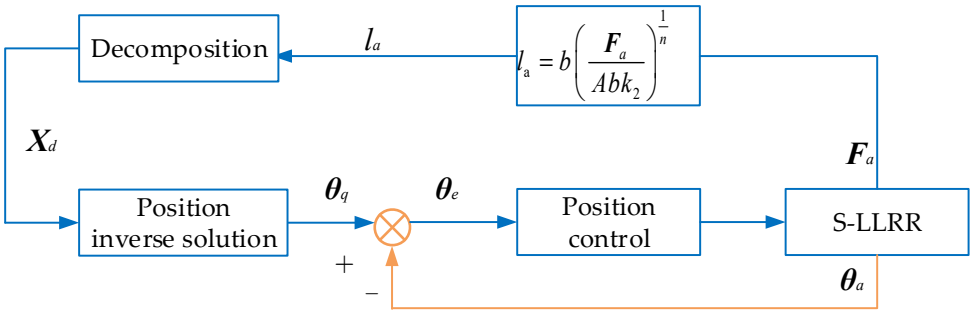


Figure 13. Block diagram of active control strategy for rehabilitation robot.

3.4. Evaluation of Active Participation Based on Physiological Signals

The degree of patient participation in active training is closely related to the rehabilitation effect, and the degree of fatigue is the direct manifestation of their willingness to actively participate in training [33]. This paper proposed a physiological signal-based active participation degree evaluation model using SVM, as shown in Figure 14. The main process is to incorporate the physiological information data such as surface electromyography (sEMG), electrodermal activity (EDA), electrocardiogram (ECG), and respiratory rate (RESP) collected in the early stage into the training set, and then import them into the SVM classification model for sample training after preprocessing, and calibrate the parameters according to the real values obtained from the quantitative indicators of fatigue evaluation. The quantitative indicators of fatigue degree evaluation were obtained statistically from the preliminary questionnaire survey. After completing the corresponding training, the physiological information data collected at the later stage is used as the test set and imported into the SVM regression model for regression prediction through the steps of feature extraction and screening. The output prediction results can be compared with the quantitative indicators of fatigue degree evaluation to determine the accuracy of the evaluation model.

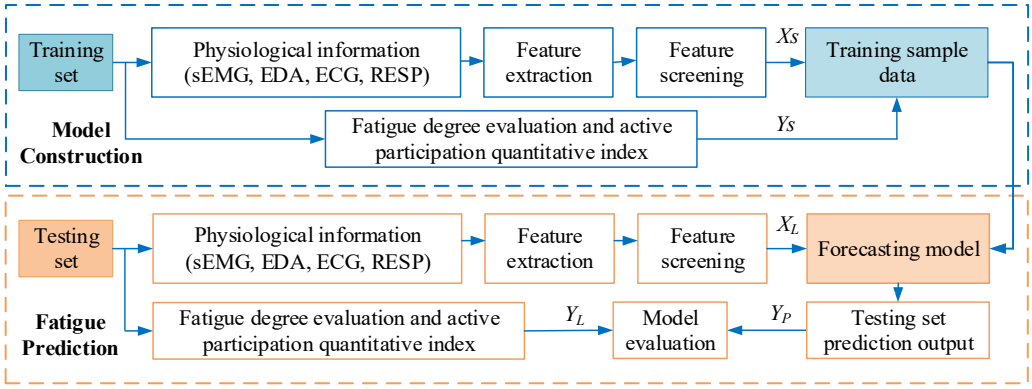


Figure 14. Active participation evaluation model.

To simplify the difficulty of learning the prediction model and improve the learning efficiency, the corresponding features were extracted from the sEMG signal, ECG signal, EDA signal, and RESP signal, so that the extracted features can clearly reflect the fluctuation of the signal data of volunteers during the training process [34]. For example, when fatigue occurs, the integral EMG feature (iEMG) of the sEMG signal represents the total amount of motor unit discharge when the muscle is involved at a certain time, reflecting the strength of the muscle's EMG activity over a period of time. Additionally, the RMS characteristic is the amplitude of the surface EMG. With the deepening of fatigue, the amplitude of the surface EMG signal will increase. The ECG signal is analyzed in the time domain by calculating the standard deviation (SDNN) of the N-N interval and the root mean square deviation (RMSSD) of the difference between adjacent N-N intervals. The gradient level skin conductance level (SCL) variation of the EDA signal is analyzed, and the SCLMean, standard deviation (SCLSTD), and polar distance (SCLPD) are extracted from this signal, SCLPD, and other features. For the RESP signal, features such as respiratory RESPMean and RESPSTD are extracted from the signal. Some of the physiological signal features used in this paper are calculated as shown in Table 2.

Table 2. Physiological signal characteristics calculation formula.

Features	Equations
SDNN	$\mathrm{SDNN} = \sqrt{\frac{1}{n}\sum_{i=1}^{n}\left(RR_i - \overline{RR}\right)^2}$
RMSSD	$\mathrm{RMSSD} = \sqrt{\frac{1}{n-1}\sum_{i=1}^{n-1}\left(RR_{i+1} - RR_i\right)^2}$
iEMG	$\mathrm{iEMG} = \int_0^T x(t)dt$
RMS	$\mathrm{RMS} = \sqrt{\frac{1}{N}\sum_{i=1}^{N} x_i^2}$

The above characteristics induced by different levels of difficulty training are statistically analyzed, and the significance test is performed by a t-test analysis. The fatigue evaluation scores of the volunteers are divided into three levels: "relaxed", "moderate", and "fatigue", and the fatigue evaluation is set to a 10-point scale, in which the score of the "relaxed" state is "1~3", the score of "moderate" state is "4~7", and the score of "fatigue" state is "8~10". The data features in different difficulty training tasks are compared among the three difficulty evaluation categories of "relaxed", "moderate", and "fatigue" to select the features that can clearly distinguish the different difficulty evaluations from the above features. The features that are not significant will be further analyzed to verify whether there is a correlation between the features and the fatigue level of volunteers, and if there is a correlation, they would still be used as input parameters for the volunteer fatigue level prediction model.

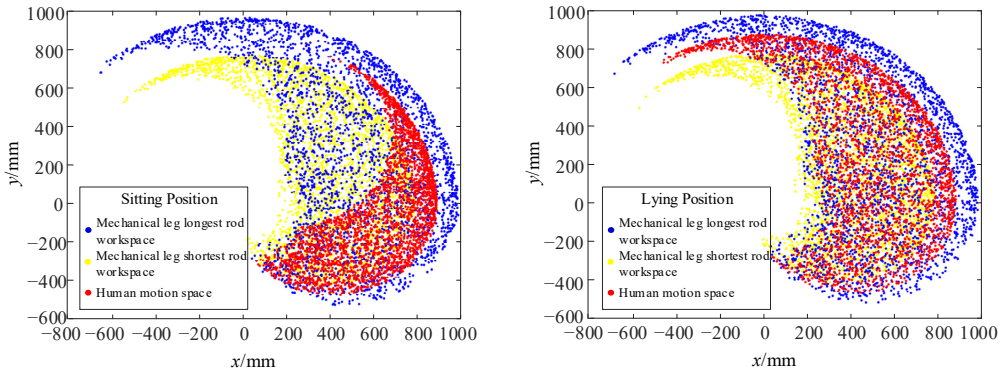
4. System Verification and Performance Analysis

To evaluate the kinematics performance of the S-LLRR, the boundary workspaces of the rehabilitation robot in sitting and lying positions were first analyzed and later compared with the length and range of motion of the human lower limbs to determine whether the workspace of the S-LLRR meets the requirements of human rehabilitation training. The length ranges of the thigh, calf, and ankle-foot parts of the human lower limbs and the angle change ranges of each joint during training in sitting and lying positions were defined, as shown in Table 3.

Table 3. Parameters of human lower-limb movement.

Unit	Length/mm	The Range of Joint Variables in Sitting Posture/°	The Range of Joint Variables in Lying Posture/°
thigh	360~460	0~60	0~125
calf	320~420	−140~0	−140~0
ankle-foot	100	−30~45	−30~45

The creation of the S-LLRR mechanical leg model and the definition of the parameters were completed in Section 3. The workspaces of the robot and the patient were obtained using the Monte Carlo method, as shown in Figure 15. The blue part of the figure is the longest rod workspace of the mechanical leg, the yellow part is the shortest rod workspace of the mechanical leg, and the red is the accessible space of the patient, which shows that the red area is enveloped in the whole and can meet the training demand of the patient.



(**a**) (**b**)

Figure 15. Patient and robot workspaces. (**a**) The workspace of sitting position. (**b**) The workspace of lying position.

Next, the S-LLRR prototype was constructed, as shown in Figure 16. To evaluate the manipulation performance of the S-LLRR, end-trajectory tracking experiments, using a GTS laser tracker, were conducted to evaluate the accuracy of its end trajectory. Three healthy volunteers were used for the experiments, and the physical status and basic information of the volunteers are shown in Table 4. The CPM rehabilitation training track was set according to the LabVIEW platform. Volunteers perform a linear passive rehabilitation exercise with a stroke of 500 mm, as shown in Figure 17. Additionally, the end trajectories were recorded and analyzed.

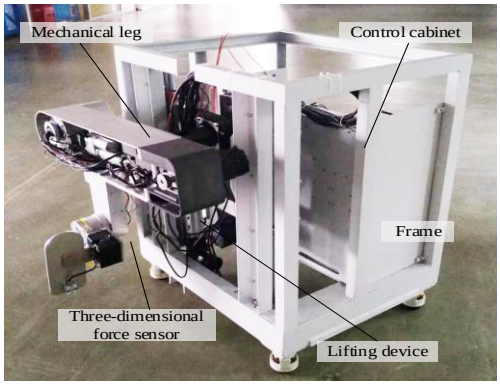


Figure 16. The S-LLRR prototype.

Table 4. Body parameters of three volunteers.

No.	Sexuality	Height/cm	Thigh Length/mm	Calf Length/mm	Weight/kg
1	male	170	460	425	68
2	male	189	530	500	65
3	female	156	410	350	48



Figure 17. End-trajectory tracking experiment.

Establish a coordinate system on the sagittal plane of the human body, with the end movement stroke as the horizontal axis and the height change as the vertical axis. As shown in Figure 18, the blue continuous line represents the theoretical end trajectory, while the orange, blue, and red dashed lines represent the end trajectories of three volunteers during the rehabilitation exercise. During the experiment, the height of the ankle joint of the mechanical leg was 139 mm, so the theoretical trajectory is a horizontal line with a height of 139 mm. The three experimental curves were relatively smooth, and the fluctuation along the y-axis was all within the range of 137.5~141 mm. The red curve had the smallest error fluctuation and was always less than 1.2 mm. Additionally, the orange curve has the largest fluctuation range, with a maximum error of 2 mm. Due to the insufficient machining accuracy of the mechanical leg, when a person gets on the machine, the end motion trajectory is mostly below the theoretical trajectory due to gravity. After halfway through the stroke, due to the knee-lifting action driving the lower limb to move upward, the trajectory of the end movement is mostly above the theoretical trajectory. The posture near the starting point and the end fluctuates greatly due to inertia and torque, so the beginning and the end of the trajectory curve are not completely coincidental. Overall, the end trajectory experiment fluctuates within an acceptable range, proving that the prototype runs relatively well.

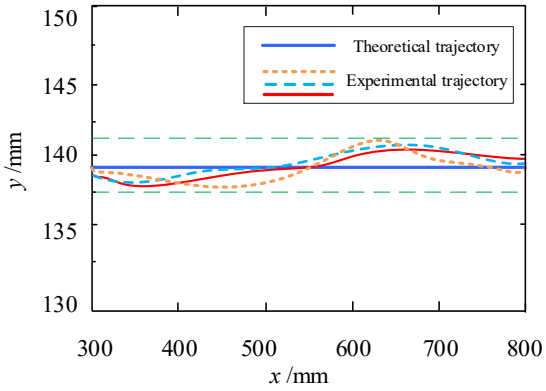


Figure 18. Experimental data analysis of End-trajectory tracking.

To verify the validity of the active participation degree evaluation model, 19 healthy volunteers were recruited for this paper to perform 35 sets of CPM training movements with different leg weights and different frequencies, respectively. The human factors engineering ErgoLABb smart wearable human factors recorder developed by Beijing Jinfa Technology Company was used in the experiment to collect the physiological signals of the volunteers. The hardware part contains an electrode sheet-type EMG signal acquisition sensor, an ECG signal acquisition sensor, a finger-end skin electrical signal acquisition sensor, a lapband breathing acquisition sensor, and a signal transmission base station, and the software part contains an ErgoLAB signal display and a postprocessing upper computer, etc. Disposable electrodes with a solid gel as a conductive gel were used for EMG signal acquisition from the quadriceps muscle. Two acquisition electrodes were placed at the bulge of the thigh muscle with a center distance of 20~30 mm, and the reference electrode was glued to the knee joint bony prominence as the neutral end of the signal. The placement of the information acquisition device is shown in Figure 19.

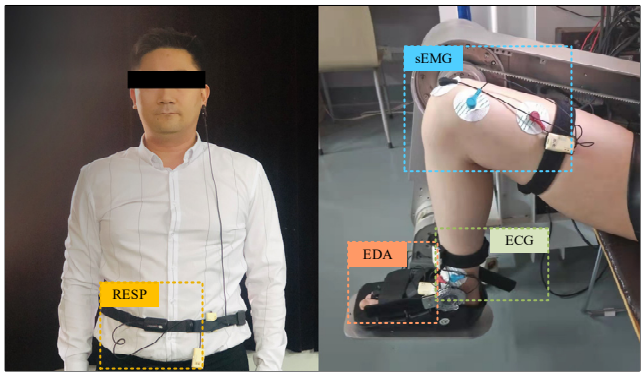


Figure 19. Physiological signal acquisition sensor and its position.

Before the acquisition, the corresponding thigh quadriceps, earlobe, toe, and abdomen areas were wiped with 75% alcohol to remove surface oil and reduce contact impedance, and then the wireless module was worn on the corresponding location of the volunteer acquisition signal. The experimental configuration of the acquisition channels is shown in Table 5.

Table 5. Experimental configuration of the acquisition channel.

Object	Position	RF Channel	Sampling Rate	Magnification
sEMG	quadriceps	2.44 GHz	2048 Hz	2000
ECG	ear lobe	2.44 GHz	512 Hz	2000
EDA	toe	2.44 GHz	64 Hz	2000
RESP	abdomen	2.44 GHz	64 Hz	2000

During the experiment, each healthy volunteer was asked to sit in front of a collection device and perform a CPM training task with a weight of 2~8 kg according to the on-screen prompts and was required to complete 2~10 repetitions per minute, respectively, and each training task was performed for 20 min. At the end of the training task, each volunteer was asked to complete a questionnaire to determine their subjective level of physical fatigue after participating in the training task, with fatigue scores increasing from 1 to 10. These physiological signals were collected throughout the experiment, and a total of 665 sets of data were obtained. After processing these sample data using the method described in Section 3.4, the feature amount was used as the input parameter $\boldsymbol{X}_s$ of the training sample set, and the questionnaire results of 19 volunteers for different difficulty tasks were used as the output of the known category information $\boldsymbol{Y}_s$ of the training set. After that, the 10 volunteers were selected to train in two groups of random difficulty tasks again, and questionnaire surveys were conducted after the training. Then, the feature quantity of 20 sets of training data was generated as the prediction sample input $\boldsymbol{X}_l$. At the same time, a questionnaire survey was conducted on 10 volunteers, and the task training difficulty evaluation was used as the real output value of the prediction sample $\boldsymbol{Y}_l$. The active participation degree evaluation model was trained by the training data $\boldsymbol{X}_s$ and $\boldsymbol{Y}_s$, and the active participation degree evaluation was established in accordance with the model, and finally, $\boldsymbol{X}_l$ was used as the input of the trained model to obtain the predicted output $\boldsymbol{Y}_p$. The actual and predicted values of the predicted sample data were analyzed, as shown in Figure 20. As described in Section 3.4, the fatigue evaluation based on the 10 points is divided into three states: "fatigue", "moderate", and "relaxed". The "fatigue" state is set to "1", the "comfortable" state is set to "0", and the "relaxed" state is set to "−1". The training data of the known 20 groups of volunteers were evaluated for three difficulties of "−1", "0", and "1". Since volunteers have different evaluation criteria for task difficulty, the results were distributed around three values to reduce this difference. The results after the algorithm test were distributed near the three difficulty values. The interval corresponding to the difficulty evaluation of "−1" is [−1.25, −0.25], the interval corresponding to the difficulty evaluation of "0" is (−0.25, 0.25], and the interval corresponding to the difficulty evaluation of "1" is (0.25, 1.25].

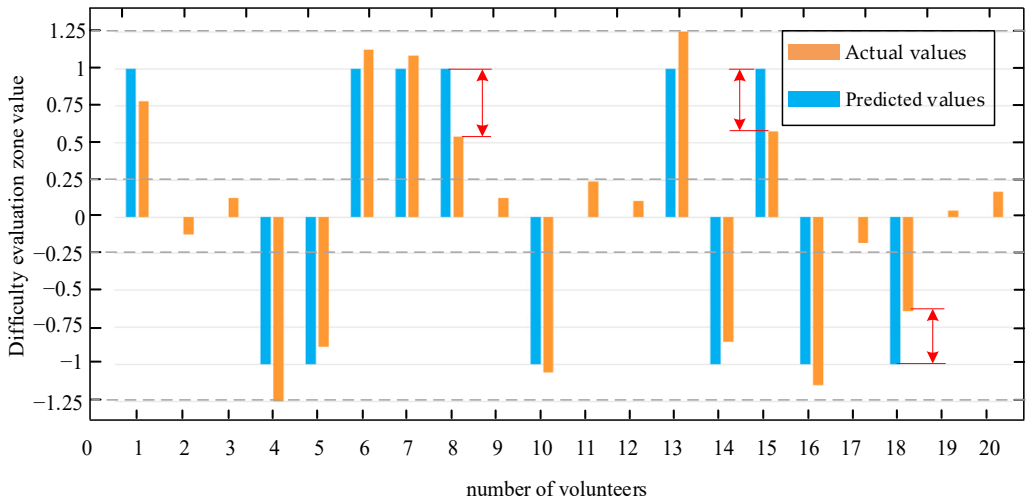


Figure 20. Comparison of predicted and real values of task difficulty prediction.

The different colors in Figure 20 represent the actual values of the volunteers and the predicted values of the model. Observe whether the absolute value of the difference between the different colors in each group is within 0.25. Exceeding this value is deemed as deviation, and the opposite is correct. Therefore, the true value of 3 out of 20 sets of data deviated from the predicted value, and the accuracy of the test reached 85%. In the experiment, the accuracy of human physiological signal acquisition was related to the

deviation of patch sensitivity and paste position, and to the emotional fluctuation, mental state, and laboratory temperature of the volunteers during the experiment. This result proves that the evaluation of the difficulty of rehabilitation training of volunteers can be obtained from the data, and the evaluation model of the degree of active participation of the lower-limb rehabilitation robot has a high accuracy rate.

5. Conclusions and Future Work

This paper proposes a new single-leg lower-limb rehabilitation robot with a simple structure and convenient movement that can adapt to different vehicle heights and lower-limb lengths of patients and be used in different rehabilitation stages, especially for the lower-limb rehabilitation needs of early patients when it is inconvenient to move. The main conclusions are as follows:

(1) For the S-LLRR, the end position of the mechanical leg was calculated first, then the trajectory planning based on CPM training mode was carried out and the curves of the rotation angle, angular velocity, and angular acceleration of the hip joint and knee joint were simulated. Through the above analysis, the rationality of mechanism design and trajectory planning was proven.

(2) The workspace of S-LLRR was simulated and analyzed, proving that it could meet the training needs of patients. The prototype system was built, and the end-track tracking of the experiment showed that the fluctuation along the Y-axis is all within the range of 137.5–141 mm and error was less than 2 mm compared with the preset value, proving that S-LLRR achieved relatively high motion accuracy.

(3) The patient fatigue test was carried out using the evaluation model of active participation based on physiological signals, and the accuracy rate of fatigue prediction reached 85%, which proved that the evaluation model of active participation has a high accuracy rate. It can be used as an evaluation standard for the rehabilitation performance of S-LLRR active training, and as a basis for medical students to formulate training plans for patients.

In future work, the structural design and control methods of S-LLRR will be further optimized, and clinical trials will be conducted to verify the effectiveness of active training and rehabilitation after the function is completed. The active participation evaluation model mentioned in the paper can only be used for the formulation of training plans. Therefore, consideration will be given to combining human physiological information with control methods to better achieve human-computer interaction.

Author Contributions: Methodology, H.Y. and S.Z. (Siyuan Zheng); Conceptualization, H.Y. and L.S.; Literature re-trieval, S.Z. (Shuo Zhang) and Z.Q.; Research design, H.Y. and S.Z. (Siyuan Zheng); Software, J.W. and S.Z. (Shuo Zhang); Data collection, Y.C. and S.Z. (Shuo Zhang); Chart making, H.Y. and J.W.; Validation, S.Z.(Siyuan Zheng), Y.C. and Z.Q.; Writing—original draft preparation, H.Y., S.Z. (Siyuan Zheng), and J.W.; Writing—review and editing, L.S. and Y.C.; Project administration, L.S. All authors have read and agreed to the published version of the manuscript.

Funding: This research was funded by China's Science and Technology Assistance Program for Developing Countries (KY201501009) and the Key Research and Development Program of Hebei (19211820D).

Data Availability Statement: The original data contributions presented in the study are included in the article, further inquiries can be directed to the corresponding authors.

Conflicts of Interest: The authors declare no conflict of interest.

References

1. Feigin, V.L.; Stark, B.A.; Johnson, C.O.; Roth, G.A.; Bisignano, C.; Abady, G.G.; Hamidi, S. Global, regional, and national burden of stroke and its risk factors, 1990–2019: A systematic analysis for the Global Burden of Disease Study 2019. *Lancet Neurol.* **2021**, *20*, 795–820. [CrossRef]
2. Markus, H.S. Reducing disability after stroke. *Int. J. Stroke* **2022**, *17*, 249–250. [CrossRef]

3. Zhang, F.; Hou, Z.G.; Cheng, L.; Wang, W.; Chen, Y.; Hu, J. Ileg—A lower limb rehabilitation robot: A proof of concept. *IEEE Trans. Hum.-Mach. Syst.* **2016**, *46*, 761–768. [CrossRef]
4. Stewart, S.; MacIntyre, K.; Capewell, S.; McMurray, J.J. Heart failure and the aging population: An increasing burden in the 21st century? *Heart* **2003**, *89*, 49–53. [CrossRef]
5. Flansbjer, U.B.; Holmbck, A.M.; Downham, D.; Patten, C.; Lexell, J. Reliability of gait performance in men and women with hemiparesis after stroke. *J. Rehabil. Med.* **2005**, *37*, 75–82.
6. Aurich, T.; Gut, A.; Labruyere, R. The FreeD module for the Lokomat facilitates a physiological movement pattern in healthy people—A proof of concept study. *J. Neuroeng. Rehabil.* **2019**, *16*, 1–13.
7. Akdoğan, E.; Adli, M.A. The design and control of a therapeutic exercise robot for lower limb rehabilitation: Physiotherabot. *Mechatronics* **2011**, *21*, 509–522. [CrossRef]
8. Yin, Q.; Hu, A.; Li, Q.; Wei, X.; Yang, H.; Wang, B.; Zhang, G. Compound lower limb vibration training rehabilitation robot. *Concurr. Comput. Pract. Exp.* **2021**, *33*, e6059. [CrossRef]
9. Wang, Y.; Xu, Q. Design and testing of a soft parallel robot based on pneumatic artificial muscles for wrist rehabilitation. *Sci. Rep.* **2021**, *11*, 1273. [CrossRef]
10. Wang, K.Y.; Yin, P.C.; Yang, H.P.; Tang, X.Q. The man-machine motion planning of rigid-flexible hybrid lower limb rehabilitation robot. *Adv. Mech. Eng.* **2018**, *10*, 16878140–18775865. [CrossRef]
11. Barbosa, A.M.; Carvalho, J.C.M.; Goncalves, R.S. Cable-driven lower limb rehabilitation robot. *J. Braz. Soc. Mech. Sci. Eng.* **2018**, *40*, 1–11. [CrossRef]
12. Tomisaki, H. Development of portable therapeutic exercise machine TEM LX2 type D. In *36th International Symposium on Robotics Symposium Digest*; At the Keidanren Kaikan in Tokyo; Emerald Group Publishing Limited: West Yorkshire, UK, 2005.
13. Wang, L.; Tian, J.; Du, J.; Zheng, S.; Niu, J.; Zhang, Z.; Wu, J. A hybrid mechanism-based robot for end-traction lower limb rehabilitation: Design, analysis and experimental evaluation. *Machines* **2022**, *10*, 99. [CrossRef]
14. Zhang, X.; Yue, Z.; Wang, J. Robotics in lower-limb rehabilitation after stroke. *Behav. Neurol.* **2017**, *2017*, 1–13. [CrossRef]
15. Mayetin, U.; Kucuk, S. Design and Experimental Evaluation of a Low Cost, Portable, 3-DOF Wrist Rehabilitation Robot with High Physical Human–Robot Interaction. *J. Intell. Robot. Syst.* **2022**, *106*, 65. [CrossRef]
16. Curcio, E.M.; Carbone, G. Mechatronic design of a robot for upper limb rehabilitation at home. *J. Bionic Eng.* **2021**, *18*, 857–871. [CrossRef]
17. Gallagher, J.F.; Sivan, M.; Levesley, M. Making Best Use of Home-Based Rehabilitation Robots. *Appl. Sci.* **2022**, *12*, 1996. [CrossRef]
18. Yang, Q.; Xie, C.; Tang, R.; Liu, H.; Song, R. Hybrid active control with human intention detection of an upper-limb cable-driven rehabilitation robot. *IEEE Access* **2020**, *8*, 195206–195215. [CrossRef]
19. Gui, K.; Liu, H.; Zhang, D. Toward multimodal human–robot interaction to enhance active participation of users in gait rehabilitation. *IEEE Trans. Neural Syst. Rehabil. Eng.* **2017**, *25*, 2054–2066. [CrossRef]
20. Hu, J.; Meng, Q.; Zhu, Y.; Zhang, X.; Wu, W.; Yu, H. Spring damping based control for a novel lower limb rehabilitation robot with active flexible training planning. *Technol. Health Care* **2022**, *31*, 565–578. [CrossRef]
21. Khan, M.A.; Saibene, M.; Das, R.; Brunner, I.; Puthusserypady, S. Emergence of flexible technology in developing advanced systems for post-stroke rehabilitation: A comprehensive review. *J. Neural Eng.* **2021**, *18*, 061003. [CrossRef]
22. Meng, W.; Liu, Q.; Zhou, Z.; Ai, Q. Active interaction control applied to a lower limb rehabilitation robot by using EMG recognition and impedance model. *Ind. Robot Int. J.* **2014**, *41*, 465–479. [CrossRef]
23. Sheng, B.; Tang, L.; Moosman, O.M.; Deng, C.; Xie, S.; Zhang, Y. Development of a biological signal-based evaluator for robot-assisted upper-limb rehabilitation: A pilot study. *Australas. Phys. Eng. Sci. Med.* **2019**, *42*, 789–801. [CrossRef]
24. Zhou, J.; Yang, S.; Xue, Q. Lower limb rehabilitation exoskeleton robot: A review. *Adv. Mech. Eng.* **2021**, *13*, 16878140211011862. [CrossRef]
25. Wang, X.; Liu, G.; Feng, Y.; Li, W.; Niu, J.; Gan, Z. Measurement method of human lower limb joint range of motion through human-machine interaction based on machine vision. *Front. Neurorobot.* **2021**, *15*, 753924. [CrossRef]
26. Roaas, A.; Andersson, G.B. Normal range of motion of the hip, knee and ankle joints in male subjects, 30–40 years of age. *Acta Orthop. Scand.* **1982**, *53*, 205–208. [CrossRef]
27. Beckerle, P.; Salvietti, G.; Unal, R.; Prattichizzo, D.; Rossi, S.; Castellini, C.; Bianchi, M. A human–robot interaction perspective on assistive and rehabilitation robotics. *Front. Neurorobot.* **2017**, *11*, 24. [CrossRef]
28. Grosu, V.; Grosu, S.; Vanderborght, B.; Lefeber, D.; Rodriguez-Guerrero, C. Multi-axis force sensor for human–robot interaction sensing in a rehabilitation robotic device. *Sensors* **2017**, *17*, 1294. [CrossRef]
29. Tian, J.; Wang, H.; Zheng, S.; Ning, Y.; Zhang, X.; Niu, J.; Vladareanu, L. sEMG-Based Gain-Tuned Compliance Control for the Lower Limb Rehabilitation Robot during Passive Training. *Sensors* **2022**, *22*, 7890. [CrossRef]
30. Shen, C.; Liu, F.; Yao, L.; Li, Z.; Qiu, L.; Fang, S. Effects of MOTOmed movement therapy on the mobility and activities of daily living of stroke patients with hemiplegia: A systematic review and meta-analysis. *Clin. Rehabil.* **2018**, *32*, 1569–1580. [CrossRef]
31. Noble, S.; Pearcey, G.E.; Quartly, C.; Zehr, E.P. Robot controlled, continuous passive movement of the ankle reduces spinal cord excitability in participants with spasticity: A pilot study. *Exp. Brain Res.* **2019**, *237*, 3207–3220. [CrossRef]
32. Wu, Q.; Wang, X.; Chen, B.; Wu, H. Patient-active control of a powered exoskeleton targeting upper limb rehabilitation training. *Front. Neurol.* **2018**, *9*, 817. [CrossRef] [PubMed]

33. Horton, S.; Mares, K.; Coull, N.; Poland, F. On the character and production of active participation in neuro-rehabilitation: An Actor-Network perspective. *Sociol. Health Illn.* **2017**, *39*, 1529–1541. [CrossRef] [PubMed]
34. Jahromi, M.G.; Parsaei, H.; Zamani, A.; Dehbozorgi, M. Comparative analysis of wavelet-based feature extraction for intramuscular EMG signal decomposition. *J. Biomed. Phys. Eng.* **2017**, *7*, 365.

Disclaimer/Publisher's Note: The statements, opinions and data contained in all publications are solely those of the individual author(s) and contributor(s) and not of MDPI and/or the editor(s). MDPI and/or the editor(s) disclaim responsibility for any injury to people or property resulting from any ideas, methods, instructions or products referred to in the content.